Fano effect through parallel-coupled double Coulomb islands

2006 J. Phys.: Condens. Matter 18 8961

(http://iopscience.iop.org/0953-8984/18/39/025)

INSTITUTE OF PHYSICS PUBLISHING JOURNAL OF PHYSICS: CONDENSED MATTER

J. Phys.: Condens. Matter **18** (2006) 8961–8972 doi:10.1088/0953-8984/18/39/025

Fano effect through parallel-coupled double Coulomb islands

Haizhou Lu[1], **Rong Lu**[2] **and Bang-fen Zhu**[1,2]

[1] Center for Advanced Study, Tsinghua University, Beijing 100084, People's Republic of China
[2] Department of Physics, Tsinghua University, Beijing 100084, People's Republic of China

E-mail: luhz02@mails.thu.edu.cn, rlu@mail.tsinghua.edu.cn and bfz@mail.tsinghua.edu.cn

Received 2 March 2006, in final form 28 July 2006
Published 15 September 2006
Online at stacks.iop.org/JPhysCM/18/8961

Abstract

By means of the nonequilibrium Green function and equation of motion method, the electronic transport is theoretically studied through a parallel-coupled double quantum dot (DQD) in the presence of on-dot Coulomb interaction U. With focus on the quantum interference in the U-dominant parallel-coupled DQD, we find two types of Fano interferences in the conductance spectra. If the one-particle DQD bonding and antibonding bands are well separated from their Coulomb blockade counterparts, the main features of Fano interference in usual DQD systems are recovered with minor revisions. The most interesting is the hybridization between the antibonding state and the Coulomb counterpart of the bonding state, which gives rises to two new channels for Fano resonance. The Fano interference in the Coulomb hybridized systems can be controlled by the electrostatic and magnetic approaches, and exhibits properties quite different from what are reported in the noninteracting Fano–Anderson model.

(Some figures in this article are in colour only in the electronic version)

1. Introduction

Fano resonance stems from quantum interference between resonant and nonresonant processes [1], and manifests itself in spectra as asymmetric line shape in a large variety of experiments. It is known that the Fano effect is a good probe for the phase coherence for carriers in solids, in particular in the quantum dot (QD) system [2–7]. Unlike the conventional Fano resonance [8–11], the Fano effect in the QD system has its advantage in that its key parameters can be readily tuned. The first observation of the Fano line shape in the transport properties in the QD system was reported by Göres *et al* [3, 4] in single-electron-transistor experiments. Recently, Kobayashi *et al* studied the magnetically and electrostatically tuned Fano effect in a QD embedded in an Aharonov–Bohm (AB) ring [5, 6], and Johnson *et al* investigated a tunable

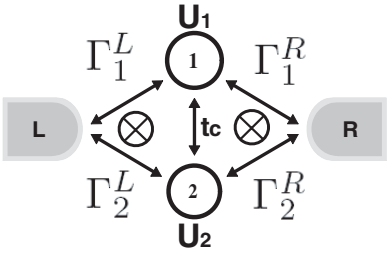

Figure 1. Schematic setup of a tunnelling-coupled parallel DCI system coupled to two reservoirs.

Fano interferometer consisting of a QD coupled to a one-dimensional channel and observed the Coulomb-modified Fano resonances [7].

Recent experimental advances in parallel-coupled double quantum dots (DQDs) [12–16], in which two QDs coupled via barrier tunnelling t_c are respectively embedded into opposite arms of a AB ring and also coupled to two leads roughly equally (cf figure 1), have inspired a number of theoretical attempts to study the coherent and correlated transport in this system [17–27]. As a controllable two-level system, it is appealing for the parallel-coupled DQD system to be a platform of investigating various quantum effects such as the Fano interference, Kondo correlation, and antiferromagnetic impurity–spin correlation. The parallel-coupled DQD system may become one of the promising candidates as the quantum bit in quantum computation based on solid state devices [28]. The entangled quantum states required for performing the quantum computation demand a high degree of phase coherence in the system [29]. Being a probe of the phase coherence [30], the Fano effect in the parallel-coupled DQD system is certainly of practical importance, especially if its swap effect can be manipulated by tuning.

The theoretical investigations of the Fano effect in the parallel-coupled DQD system can be roughly divided into two regimes, related to two sets of recent experiments, respectively [12–16].

In one recent experiment, Chen *et al* [16] studied the competition between the Kondo correlations and antiferromagnetic impurity–spin correlation. In this regime, the system can be described by the slave-boson mean field technique with infinite U or finite U. The Kondo assisted transport has been suppressed in the system due to interference between many-body quantum states [22–25], which can be understood as a generalization of the usual one-particle Fano effect.

The other set of experiments, by Holleitner *et al*, is not governed by the spin correlation effect despite the on-site Coulomb repulsions [12–14]. The reason why the Kondo correlation does not play an important role in these experiments is simply due to the fact that in these experiments the spin exchange coupling between the dot and lead states is rather weak, leading to a Kondo temperature much lower than the electron temperature. The inter-dot coupling is also weak so that the antiferromagnetic impurity–spin correlation between the two dots is smeared by the environment. In this regime, the Fano–Anderson model has been adopted in previous works, in which the electron–electron repulsion is entirely ignored [17–21], though its existence is a fact.

In this work, we intend to demonstrate that though all spin correlation is overwhelmed by the electronic temperature in experiments by Holleitner *et al*, the quantum interference together with the mean-field on-site interaction in the parallel coupled double Coulomb islands (DCIs) will lead to some interesting phenomena. We shall start with a two-impurity Anderson model

with the inter-dot tunnelling coupling t_c to describe the parallel-coupled DCI system. Within this model we shall show two types of Fano interference.

(1) If two dot levels are degenerate, the main features of the Fano interference between the resonant and nonresonant channels reported in the previous no-U model are qualitatively recovered for the Coulomb blockade counterparts, only minor revisions needed.
(2) In the presence of a finite level separation between two dots $\Delta\varepsilon$, for a system with proper inter-dot coupling and on-site U, the antibonding state may be hybridized with the Coulomb blockade of the bonding state, forming two channels.

The quantum interference between these two hybridized channels gives rise to a new-type Fano resonance. This type of Fano interference can be controlled by the level detuning and magnetic flux. We estimate that to observe it requires that the quantum dots should be of radius about 2–6 nm. This may be feasible, particularly in such single-electron devices as single-molecule transistors [31–34].

The paper is organized as follows. In section 2, after the model and formalism is introduced, a discussion is given to justify the approximation we take compared to the experimental data from [12]. Our main numerical results will be presented in section 3, in which we also suggest the experimental candidate to probe the novel phenomena. Finally, the validity of the approximation is again discussed and a brief summary is given.

2. Physical model and current formula

The model Hamiltonian (cf figure 1) is as follows:

$$H = H_{\mathrm{DQD}} + H_{\mathrm{leads}} + H_{\mathrm{T}}. \tag{1}$$

The parallel-coupled DCI system is described with the two-impurity Anderson model with an inter-dot tunnelling-coupling term as

$$H_{\mathrm{DQD}} = \sum_{i,\sigma} \varepsilon_{i\sigma} d^{\dagger}_{i\sigma} d_{i\sigma} + \sum_{i} U_i d^{\dagger}_{i\uparrow} d_{i\uparrow} d^{\dagger}_{i\downarrow} d_{i\downarrow} - t_{\mathrm{c}} \sum_{\sigma} (d^{\dagger}_{1\sigma} d_{2\sigma} + \mathrm{h.c.}), \tag{2}$$

where $d^{\dagger}_{i\sigma}$ ($d_{i\sigma}$) represents the creation (annihilation) operator for the discrete state with the energy $\varepsilon_{i\sigma}$ and spin σ ($\sigma = \uparrow, \downarrow$) in the dot i ($i = 1, 2$), which are coupled to each other via tunnelling t_{c}, and the on-dot Coulomb repulsion is described in the second term on the right hand of equation (2)[3].

The H_{leads} in equation (1) represents the noninteracting electron gas in the left (L) and right (R) leads,

$$H_{\mathrm{leads}} = \sum_{k,\alpha,\sigma} \varepsilon_{k\alpha} c^{\dagger}_{k\alpha\sigma} c_{k\alpha\sigma}, \tag{3}$$

where $c^{\dagger}_{k\alpha\sigma}$ ($c_{k\alpha\sigma}$) is the creation (annihilation) operator for a continuous state in the lead α ($\alpha = \mathrm{L}, \mathrm{R}$) with energy $\varepsilon_{k\alpha}$ and spin σ. The H_{T} in equation (1) represents the tunnelling coupling between the QD and lead electrons,

$$H_{\mathrm{T}} = \sum_{k,\alpha,\sigma,i} V_{\alpha i} d^{\dagger}_{i\sigma} c_{k\alpha\sigma} + \mathrm{h.c.}, \tag{4}$$

[3] The previous mean-field results indicate that the inter-dot Coulomb interaction U' will shift the conductance peaks significantly [38, 40, 35]. Considering that inter-dot U' is usually an order of magnitude smaller than the on-site U for typical GaAs structures used in experiments and the addition of this term makes the current formalism more complicated, it is not included in the present Hamiltonian. On the other hand, in the single-occupation regime of the DQD induced by a strong interdot repulsion, the low-energy behaviour is characterized by an $SU(4)$ Kondo effect, which has already been described by the slave boson mean-field, numerical renormalization group or Bethe ansatz exact solution [43–45]. Because of the fluctuation of the orbital degree of freedom (pseudospin), this effect is sensitive to the magnetic flux threading the DQD AB ring. When a magnetic flux other than π breaks the conservation of pseudospin quantum number, the $SU(4)$ Kondo reduces to the common $SU(2)$ Kondo with an enhanced Kondo temperature [44].

where for the sake of simplicity the tunnelling matrix element $V_{\alpha i}$ is assumed to be independent of k, and the phase shift due to the total magnetic flux threading into the AB ring, Φ, is assumed to distribute evenly among four sections of the DQD AB ring. Namely, $V_{\mathrm{L}1} = |V_{\mathrm{L}1}|\mathrm{e}^{\mathrm{i}\frac{\phi}{4}}$, $V_{\mathrm{L}2}^{*} = |V_{\mathrm{L}2}|\mathrm{e}^{\mathrm{i}\frac{\phi}{4}}$, $V_{\mathrm{R}1}^{*} = |V_{\mathrm{R}1}|\mathrm{e}^{\mathrm{i}\frac{\phi}{4}}$, and $V_{\mathrm{R}2} = |V_{\mathrm{R}2}|\mathrm{e}^{\mathrm{i}\frac{\phi}{4}}$, where $\phi = 2\pi\Phi/\Phi_0$, with the flux quantum $\Phi_0 = hc/e$. In the following calculation, we define the line-width matrix as $\Gamma_{ij}^{\alpha} \equiv \sum_k V_{\alpha i} V_{\alpha j}^{*} 2\pi\delta(\varepsilon - \varepsilon_{k\alpha})$ ($\alpha = \mathrm{L}, \mathrm{R}$) and $\mathbf{\Gamma} = \mathbf{\Gamma}^{\mathrm{L}} + \mathbf{\Gamma}^{\mathrm{R}}$. According to figure 1, the line-width matrices read

$$\mathbf{\Gamma}^{\mathrm{L/R}} = \begin{pmatrix} \Gamma_1^{\mathrm{L/R}} & \sqrt{\Gamma_1^{\mathrm{L/R}}\Gamma_2^{\mathrm{L/R}}}\,\mathrm{e}^{\pm\mathrm{i}\frac{\phi}{2}} \\ \sqrt{\Gamma_1^{\mathrm{L/R}}\Gamma_2^{\mathrm{L/R}}}\,\mathrm{e}^{\mp\mathrm{i}\frac{\phi}{2}} & \Gamma_2^{\mathrm{L/R}} \end{pmatrix}, \tag{5}$$

where Γ_i^{α} is short for Γ_{ii}^{α}.

According to Meir and Wingreen [36], the general formula for current through a mesoscopic region between two noninteracting leads is given by

$$J = \sum_{\sigma} \frac{\mathrm{i}e}{2h} \int \mathrm{d}\omega\ \mathrm{Tr}\{(\mathbf{\Gamma}^{\mathrm{L}} - \mathbf{\Gamma}^{\mathrm{R}})\mathbf{G}^{<}(\omega) + [f_{\mathrm{L}}(\omega)\mathbf{\Gamma}^{\mathrm{L}} - f_{\mathrm{R}}(\omega)\mathbf{\Gamma}^{\mathrm{R}}](\mathbf{G}^{\mathrm{r}}(\omega) - \mathbf{G}^{\mathrm{a}}(\omega))\}, \tag{6}$$

where $f_{\mathrm{L\ (R)}}(\omega)$ is the Fermi distribution function on the left (right) leads, $\mathbf{G}^{\mathrm{r}}$, $\mathbf{G}^{\mathrm{a}}$, and $\mathbf{G}^{<}$ are respectively the retarded, advanced, and lesser Green functions in the DQD region, defined as

$$\begin{aligned} G_{i\sigma,\,j\sigma}^{\mathrm{r}}(t) &\equiv \langle\langle d_{i\sigma}(t)|d_{j\sigma}^{\dagger}\rangle\rangle^{\mathrm{r}} \equiv -\mathrm{i}\theta(t)\langle\{d_{i\sigma}(t), d_{j\sigma}^{\dagger}\}\rangle, \\ G_{i\sigma,\,j\sigma}^{<}(t) &\equiv \langle\langle d_{i\sigma}(t)|d_{j\sigma}^{\dagger}\rangle\rangle^{<} \equiv \mathrm{i}\langle d_{j\sigma}^{\dagger} d_{i\sigma}(t)\rangle. \end{aligned} \tag{7}$$

Writing the equation of motion for the retarded Green function in Fourier space [37] $\langle\langle d_{i\sigma}|d_{j\sigma}^{\dagger}\rangle\rangle_{\omega}^{\mathrm{r}}$, one arrives at

$$\mathbf{G}^{\mathrm{r}}(\omega) = [1 - \mathbf{g}^{\mathrm{r}}(\omega)\mathbf{\Sigma}^{\mathrm{r}}]^{-1}\mathbf{g}^{\mathrm{r}}(\omega), \tag{8}$$

in the wide-band limit $\mathbf{\Sigma}^{\mathrm{r}} = -\frac{\mathrm{i}}{2}(\mathbf{\Gamma}^{\mathrm{L}} + \mathbf{\Gamma}^{\mathrm{R}})$, and $\mathbf{g}^{\mathrm{r}}(\omega)$ is the Green function for the isolated DCI. It is convenient to express the inverse of $\mathbf{g}^{\mathrm{r}}(\omega)$ as $[\mathbf{g}^{\mathrm{r}}(\omega)^{-1}]_{i\bar{i}} = t_{\mathrm{c}}$ ($\bar{i} = 2$ if $i = 1$, and vice versa), and

$$[\mathbf{g}^{\mathrm{r}}(\omega)^{-1}]_{ii} = \frac{(\omega - \varepsilon_{i\sigma})(\omega - \varepsilon_{i\sigma} - U_i)}{\omega - \varepsilon_{i\sigma} - U_i + U_i\langle n_{i\bar{\sigma}}\rangle} + \frac{U_i t_{\mathrm{c}}[\langle d_{i\bar{\sigma}}^{\dagger} d_{\bar{i}\bar{\sigma}}\rangle - \langle d_{\bar{i}\bar{\sigma}}^{\dagger} d_{i\bar{\sigma}}\rangle]}{\omega - \varepsilon_{i\sigma} - U_i + U_i\langle n_{i\bar{\sigma}}\rangle}, \tag{9}$$

where $\bar{\sigma} = -\sigma$, the expectation values of $\langle n_{\imath\bar{\sigma}}\rangle$ and $\langle d_{i\bar{\sigma}}^{\dagger} d_{\bar{i}\bar{\sigma}}\rangle$ can be calculated self-consistently by taking advantage of the definition of the lesser Green function

$$\langle d_{i\bar{\sigma}}^{\dagger} d_{\bar{i}\bar{\sigma}}\rangle = -\mathrm{i}\int_{-\infty}^{\infty} \frac{\mathrm{d}\omega}{2\pi}\, G_{\bar{i}\bar{\sigma},i\bar{\sigma}}^{<}(\omega). \tag{10}$$

During the deductions the following truncation rules are applied to the higher-order Green functions:

$$\begin{aligned} &\langle\langle d_{\bar{i}\sigma} n_{i\bar{\sigma}}|d_{j\sigma}^{\dagger}\rangle\rangle_{\omega}^{\mathrm{r}} \cong \langle n_{i\bar{\sigma}}\rangle\langle\langle d_{\bar{i}\sigma}|d_{j\sigma}^{\dagger}\rangle\rangle_{\omega}^{\mathrm{r}}, \\ &\langle\langle d_{i\sigma} d_{i\bar{\sigma}}^{\dagger} d_{\bar{i}\bar{\sigma}}|d_{j\sigma}^{\dagger}\rangle\rangle_{\omega}^{\mathrm{r}} \cong \langle d_{i\bar{\sigma}}^{\dagger} d_{\bar{i}\bar{\sigma}}\rangle\langle\langle d_{i\sigma}|d_{j\sigma}^{\dagger}\rangle\rangle_{\omega}^{\mathrm{r}}, \\ &\langle\langle c_{k\alpha\sigma} n_{i\bar{\sigma}}|d_{j\sigma}^{\dagger}\rangle\rangle_{\omega}^{\mathrm{r}} \cong \langle n_{i\bar{\sigma}}\rangle\langle\langle c_{k\alpha\sigma}|d_{j\sigma}^{\dagger}\rangle\rangle_{\omega}^{\mathrm{r}}, \\ &\langle\langle d_{i\bar{\sigma}}^{\dagger} c_{k\alpha\bar{\sigma}} d_{i\sigma}|d_{j\sigma}^{\dagger}\rangle\rangle_{\omega}^{\mathrm{r}} \cong \langle d_{i\bar{\sigma}}^{\dagger} c_{k\alpha\bar{\sigma}}\rangle\langle\langle d_{i\sigma}|d_{j\sigma}^{\dagger}\rangle\rangle_{\omega}^{\mathrm{r}}. \end{aligned} \tag{11}$$

By these truncations, all the inter-dot and dot–lead spin-flip correlations are ignored, and the Kondo effect is certainly beyond our considerations. Hence the electrons of opposite spin $\bar{\sigma}$ can be treated as static entities which affect the effective site energy of the electrons of spin σ through the on-site repulsion. Consequently, we have $\mathbf{G}^{<} = \mathbf{G}^{\mathrm{r}}\mathbf{\Sigma}^{<}\mathbf{G}^{\mathrm{a}}$, where

$\mathbf{\Sigma}^{<} = \mathrm{i}(f_{\mathrm{L}}\mathbf{\Gamma}^{\mathrm{L}} + f_{\mathrm{R}}\mathbf{\Gamma}^{\mathrm{R}})$ [38]. In general $\mathbf{G}^{\mathrm{r}} - \mathbf{G}^{\mathrm{a}} = \mathbf{G}^{\mathrm{r}}(\mathbf{\Sigma}^{\mathrm{r}} - \mathbf{\Sigma}^{\mathrm{a}})\mathbf{G}^{\mathrm{a}}$. Thus equation (6) of current is reduced to a usual Landauer–Büttiker formula for the noninteracting electrons [36]

$$J = \sum_{\sigma} \frac{e}{h} \int \mathrm{d}\omega \, [f_{\mathrm{L}}(\omega) - f_{\mathrm{R}}(\omega)] \, \mathrm{Tr}[\mathbf{G}^{\mathrm{a}}(\omega)\mathbf{\Gamma}^{\mathrm{R}}\mathbf{G}^{\mathrm{r}}(\omega)\mathbf{\Gamma}^{\mathrm{L}}], \tag{12}$$

implying that by ignoring all spin-flip processes the effect of electrons with spin $\bar{\sigma}$ on the motion of the electron with spin σ behaves like a background, and the coherent tunnelling process takes place between electrons with the same spin.

It must be noted that the current truncation rules work well only when the first-order direct charge transfer is allowed [27, 38–40]. In the Coulomb blockade regime, Kondo physics is expected to occur at temperatures lower than the Kondo temperature T_{K}. In the experiments by Holleitner *et al*, however, both dots are weakly coupled to the leads, leading to a Kondo temperature lower than the bath temperature. As a result, it is reasonable to ignore the Kondo effect as we do in the present work. Besides, when a large intra-dot Coulomb repulsion prevents the electrons in dots from direct hopping, the low-energy effective interaction between them is equivalent to the Heisenberg Hamiltonian $J\vec{S}1\cdot\vec{S}2$, where $J = 4tc^2/U$ comes from the second-order virtual excitations. With the parameters measured in experiments by Holleitner *et al* [12] $U = 3.36$–3.42 meV, $t_{\mathrm{c}} = 49.5$–66 μeV, and $T = (118 \pm 8)$ μK or 9.46–10.84 μeV, we estimate the antiferromagnetic exchange energy as $J = 3$–5 μeV, less than $k_{\mathrm{B}}T/2$, implying that the spin singlet–triplet spectrum structure due to the inter-dot coupling is smeared out by $k_{\mathrm{B}}T$ broadening of the Fermi surfaces in the leads. In this context, it is safe to rule out the inter-dot spin exchange process in analysing the experiments at $k_{\mathrm{B}}T > 4t_{\mathrm{c}}^2/U$. On the other hand, to observe Fano resonances in the experiment of an AB ring with one dot embedded, the temperature should be lower than around 400 mK [6]. Thus to investigate the Fano interference in DCI taking no account of the the inter-dot spin correlation, the parameters are restricted to $\Gamma > k_{\mathrm{B}}T > 4t_{\mathrm{c}}^2/U$ as in sections 3.1 and 3.2. Meanwhile, in section 3.3 a detuning between two dot levels can overcome the on-site U barrier somewhat and the requirement $4t_{\mathrm{c}}^2/U < k_{\mathrm{B}}T$ is relaxed in this case.

3. Numerical results

As pointed out in [17], in the parallel-coupled geometry, if $\Gamma_1^{\mathrm{L}} = \Gamma_2^{\mathrm{L}}$ and $\Gamma_1^{\mathrm{R}} = \Gamma_2^{\mathrm{R}}$, the antibonding state could be decoupled entirely from the leads. Our calculation verifies that this property is retained when the on-dot Coulomb repulsion is included. In the following we will only consider the following two configurations: (1) $\Gamma_1^{\mathrm{L}} = \Gamma_2^{\mathrm{R}} > \Gamma_2^{\mathrm{L}} = \Gamma_1^{\mathrm{R}}$, and (2) $\Gamma_1^{\mathrm{L}} = \Gamma_1^{\mathrm{R}} > \Gamma_2^{\mathrm{L}} = \Gamma_2^{\mathrm{R}}$. It should be pointed out that the numerical results presented in this section, though they are calculated at zero temperature, are valid only at temperature above the Kondo temperature, as all the spin-flip processes have been neglected as mentioned above.

3.1. Spectra in dominant U

We are particularly interested in how the states in the DQD region are modified by the on-dot Coulomb repulsion, and how this modification influences transport properties. For simplicity, in this subsection we first estimate the eigenstate and eigenenergy of the isolated DQD system under the condition of $U \gg t_{\mathrm{c}}$ and $\Delta\varepsilon = 0$.

If there is only one electron in the DQD system, due to the inter-dot coupling, the DQD state is the linear combination of the states in two dots, thus-formed bonding and antibonding

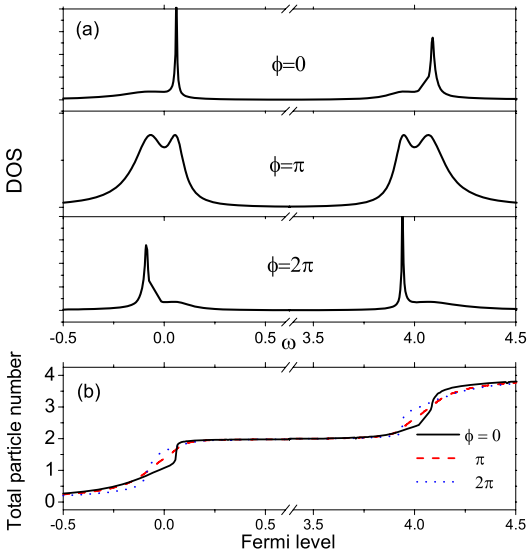

Figure 2. (a) The local density of states and (b) the total particle number in the DQD structure for different magnetic phase parameters ϕ. A magnetic flux threading into the AB ring swaps the effective couplings of the DQD states as well as their Coulomb counterparts to the leads. The parameters taken are $\varepsilon_{1\sigma} = \varepsilon_{2\sigma} = 0$, $U_1 = U_2 = 4$, $t_c = 0.1$, and $k_B T = 0.01$. For configuration 1, $\Gamma_1^L = \Gamma_2^R = 0.15$, $\Gamma_1^R = \Gamma_2^L = 0.05$; and for configuration 2, $\Gamma_1^L = \Gamma_1^R = 0.15$, $\Gamma_2^L = \Gamma_2^R = 0.05$.

states are associated with energy at $\varepsilon_0 - t_c$ and $\varepsilon_0 + t_c$, respectively. Hence, the one-electron ground state of the DQD is the bonding state with eigenenergy $\varepsilon_0 - t_c$.[4]

When the DQD contains two electrons, six possible states in the system include $|\uparrow\rangle_1|\uparrow\rangle_2$, $|\downarrow\rangle_1|\downarrow\rangle_2$, $|\uparrow\rangle_1|\downarrow\rangle_2$, $|\downarrow\rangle_1|\uparrow\rangle_2$, $|\uparrow\downarrow\rangle_1|0\rangle_2$, and $|0\rangle_1|\uparrow\downarrow\rangle_2$. The ground and excited two-electron states are determined by directly diagonalizing the matrix of $H_{\rm DQD}$ in the Hilbert space spanned by these six states. Thus the two-electron ground state has energy at $2\varepsilon_0 + \frac{1}{2}(U - \sqrt{U^2 + 16t_c^2})$, which, if $U \gg t_c$, reduces to $2\varepsilon_0 - 4t_c^2/U \sim 2\varepsilon_0$. Since the intra-dot Coulomb interaction produces effective charging energy on the bonding and antibonding states, it is expected for the two-electron ground state that the electrons tend to distribute themselves evenly throughout the DQD structure to avoid the charging energy. Since the extra charging energy has to be consumed when adding the third or the fourth electron into the system, the ground state energy is approximately equal to $3\varepsilon_0 + U - t_c$ and $4\varepsilon_0 + 2U$, respectively.

When an isolated DCI is connected to two leads, the coupling between a DCI level and leads results in broadening of the discrete level and forming the band. The local density of states (DOS), defined as the imaginary part of the retarded Green function $\rho_\sigma = -\frac{1}{\pi}\sum_{i=1,2} \mathrm{Im}\, G^r_{i\sigma,i\sigma}$, has then been calculated. The low-temperature transport properties that we are interested in are mainly determined by the electrons around the Fermi level. In the present case, the retarded Green function depends on the occupancy of electrons in dots, which is ultimately decided by the Fermi level. Hence the calculated DOS spectrum at energy ω shown in figure 2(a) is associated with the Fermi level taken also at ω.

The effective coupling between the DCI states and leads can be tuned by both the dot–lead coupling strength and the total magnetic flux. Our calculation reveals that the line shape of the local DOS critically depends on magnetic flux ϕ threading into the AB ring. As shown in

[4] Throughout this paper the bonding and antibonding states are cited in the absence of the magnetic flux. As shown in [21], the applied magnetic flux will change the order of the levels.

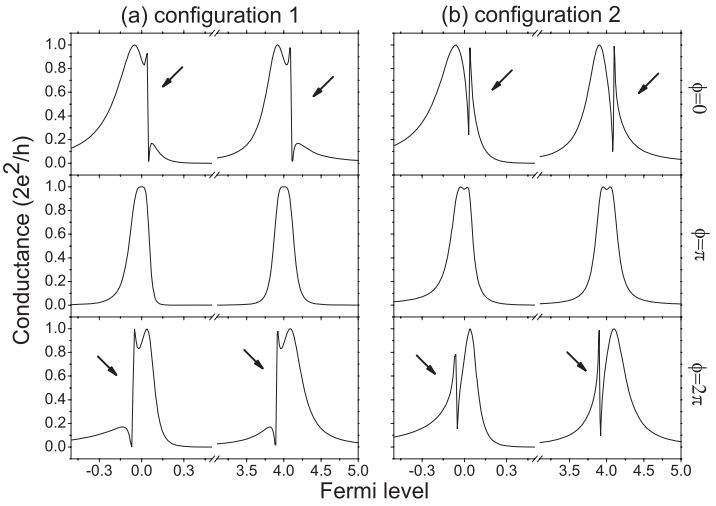

Figure 3. The differential conductances for (a) configuration 1 and (b) configuration 2 as functions of Fermi level. The Fano resonances are marked with arrows. The parameters taken are $\varepsilon_{1\sigma} = \varepsilon_{2\sigma} = 0$, $U_1 = U_2 = 4$, $t_c = 0.1$ and $k_B T = 0.01$. For configuration 1, $\Gamma_1^L = \Gamma_2^R = 0.15$, $\Gamma_1^R = \Gamma_2^L = 0.05$; and for configuration 2, $\Gamma_1^L = \Gamma_1^R = 0.15$, and $\Gamma_2^L = \Gamma_2^R = 0.05$.

figure 2(a), the band widths respond to magnetic flux ϕ according to the following rule: the broadening of the bonding band is always accompanied by shrinking the antibonding band, and similarly for their Coulomb counterparts, though the line shape is somewhat different. It should be noted from the figure that, unlike the no-U case [17–20], where the sum of the widths of the bonding and antibonding bands is invariant because the self-energy is solely determined by the DQD–lead coupling, with the on-dot U taken into consideration an additional self-energy due to the Coulomb repulsion plays a role, then the total band width in general depends on the magnetic flux ϕ to some extent. When Fermi level varies, the occupation number of electrons in the DQD region is changed correspondingly. As shown in figure 2(b), the integer number of electrons confined to the DQD region occurs approximately at the following energies: $\varepsilon_0 - t_c$, $\varepsilon_0 + t_c$, $\varepsilon_0 + U - t_c$, $\varepsilon_0 + U + t_c$ [41].

3.2. Fano effect in separated bands

Now let us consider the case in which the bonding as well as antibonding bands are well separated from their Coulomb counterparts in the situation of $U \gg t_c$ and $\Delta\varepsilon \approx 0$.

Figure 3 shows the differential conductance (defined as $\partial J/\partial V|_{V\to 0}$) as functions of the Fermi level, or equivalently the average of two dot levels. The peaks marked with arrows in the conductance spectra in two configurations represent the Fano-type peaks associated with the asymmetric line shape, compared with the symmetric Lorentzian at the same spectra. As shown in the figures and discussed in [21], the spectra vary with the magnetic flux. There are only two Lorentzian and two Fano peaks in the conductance spectra for $\phi = 0$ or 2π, while four Lorentzian peaks appear when $\phi = \pi$. The spectrum for $\phi = 2\pi$ has a mirror symmetry with that for $\phi = 0$.

In general, the bonding and antibonding states couple to lead states with different strengths, leading to different broadenings. If the band width of the strongly coupled level covers the weakly coupled band and the phase of states in the strongly coupled channel shifts little in the close vicinity of the weakly coupled level, then the Fano interference will occur at this

energy region. Here the weakly coupled channel acts as a Breit–Wigner scatterer in the resonant tunnelling process, while the strongly coupled channel can be regarded as a nonresonant one. It should be noted that in the present system the resonant or nonresonant channel is not fixed; on the contrary, it could be any one of the four channels, as long as the magnetic flux as well as the Fermi level fit it.

Notice also that when the dot–lead coupling strength is adjusted such that configuration 1 is transformed into configuration 2, as shown in figure 3, the tail direction of the Fano peak in the conductance spectra is flipped. The reason for this behaviour is that, compared to configuration 2, an extra flux of π threads into the loop in configuration 1 [21]. Thus, the Fano lineshape in configuration 1 is just opposite to that in configuration 2, i.e. if two channels interfere with each other constructively in configuration 1, then destructively in configuration 2, and vice versa.

3.3. Fano effect in hybridized bands

Interesting results appear when the separation between two dot levels, $\Delta\varepsilon$, is comparable with the on-dot U, so that the hybridization may occur between the antibonding band and the Coulomb blockade counterpart of the bonding band.

Without the hybridization, the conductance peaks associated with the bonding and antibonding bands are respectively located at $\varepsilon_0 \pm \sqrt{(\Delta\varepsilon)^2/4 + t_c^2}$. When $\Delta\varepsilon$ grows from zero, there will be a red-shift for the bonding band peak and a blue-shift for the antibonding band peak with respect to ε_0. So the separation between the two peaks is proportional to $\sqrt{(\Delta\varepsilon)^2 + 4t_c^2}$. A similar trend has also been found for their Coulomb counterparts except for a whole band shift by U. Thus, as shown in figure 4, when $\Delta\varepsilon$ increases, the antibonding peak (the second peak) and the Coulomb counterpart of the bonding peak (the third peak) in the conductance spectra will come closer. At certain values of $\Delta\varepsilon$, the two bands begin to overlap. Finally, the anticrossing region for these two peaks is reached at $\varepsilon_0 + \sqrt{(\Delta\varepsilon)^2/4 + t_c^2} \approx U + \varepsilon_0 - \sqrt{(\Delta\varepsilon)^2/4 + t_c^2}$, or $\sqrt{(\Delta\varepsilon)^2 + 4t_c^2} \approx U$. If $\Delta\varepsilon \gg t_c$, the anticrossing region is just around the Hubbard gap, $\Delta\varepsilon \approx U$. This is clearly depicted in three panels of figure 4 with different U. It should be pointed out that, as highlighted by the dashed lines in figure 4, the second and third peaks do anticross rather than cross each other around this transition region, where the two bands hybrid and overlap. The anticrossing feature is also verified by careful calculations with different parameters.

The hybridization between the second and third bands reshapes the conductance spectra. Let us take a look at the variation of the line shape in configuration 2 by comparing two spectra around the anticrossing region at U, i.e. figure 5 ($\Delta\varepsilon < U$) with figure 6 ($\Delta\varepsilon > U$).

We denote two peaks of the hybridized bands in the transition zone as peak $2'$ and peak $3'$, respectively. In figure 5, peak $2'$, associated with the antibonding band, contains more $|\mathrm{QD1}\rangle$ component and less $|\mathrm{QD2}\rangle$ component, while peak $3'$ (the Coulomb counterpart of bonding band) is related more to $|\mathrm{QD2}\rangle$. In configuration 2, QD1 couples to leads more strongly than QD2 does. Hence, with increasing $\Delta\varepsilon$ (but before the anticrossing minimum), the coupling between peak $2'$ and the leads becomes stronger and the band is broadened; on the other hand, peak $3'$, associated with a weakly coupled channel, is narrowed, even decoupled entirely from the spectra at the anticrossing minimum. When the narrow weakly coupled channel $3'$ is entirely merged into the wider band $2'$, a new Fano interference is expected to occur at the energy of peak $3'$. When $\Delta\varepsilon$ exceeds the anticrossing minimum, the main components of the second and the third channel are exchanged; $3'$ becomes the strongly coupled one gradually, and distorts $2'$ into the Fano peak (figure 6).

Besides, we notice that the broadening of $2'$ ($\Delta\varepsilon < U$) or $3'$ ($\Delta\varepsilon > U$) is always accompanied by shrinking the first peaks (the furthest left white area in figure 4), which of

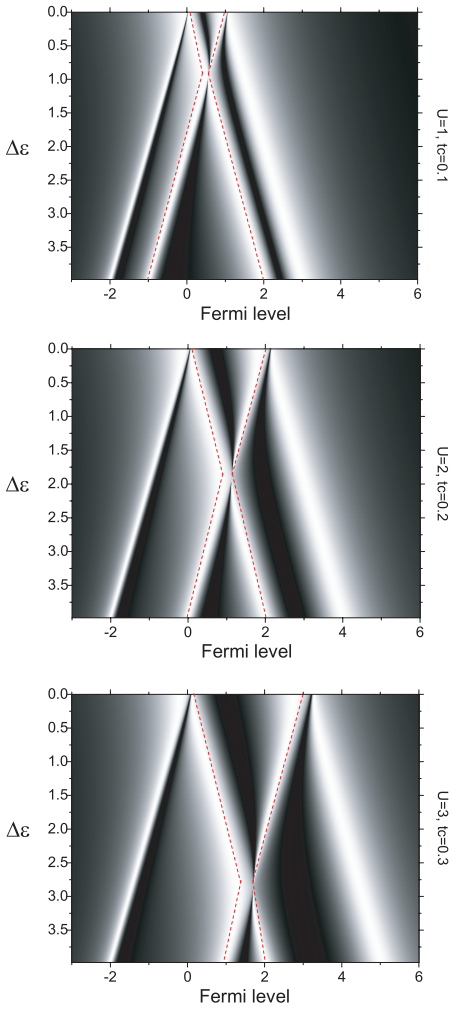

Figure 4. The conductance spectra in configuration 2 as functions of $\Delta\varepsilon$ and Fermi level for $U = 1, t_c = 0.1$; $U = 2, t_c = 0.2$; and $U = 3, t_c = 0.3$. The other parameters are taken as $\varepsilon_0 = 0$, $\Gamma_1^L = \Gamma_1^R = 1$, and $\Gamma_2^L = \Gamma_2^R = 0.15$.

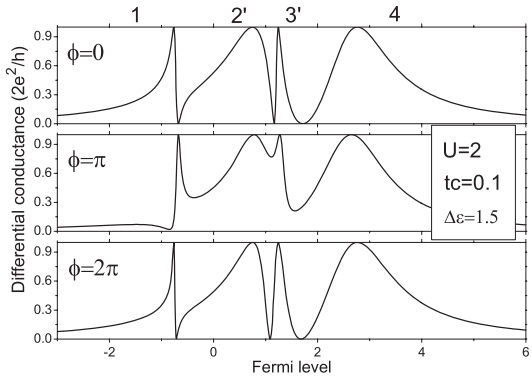

Figure 5. The conductance spectra versus Fermi level for $\Delta\varepsilon = 1.5$, $t_c = 0.1$, and $U = 2$. From top to bottom, $\phi = 4n\pi$, $(2n+1)\pi$, and $(2n+1)2\pi$. The other parameters taken for calculation are the same as figure 4.

course turns out to be the Fano resonance. The reason for the shrinking of the first channel is the reduced $|QD1\rangle$ component, quite similar to the mechanism for narrowing its Coulomb counterpart. It has to be pointed out that the phenomenon above, though expected in terms of

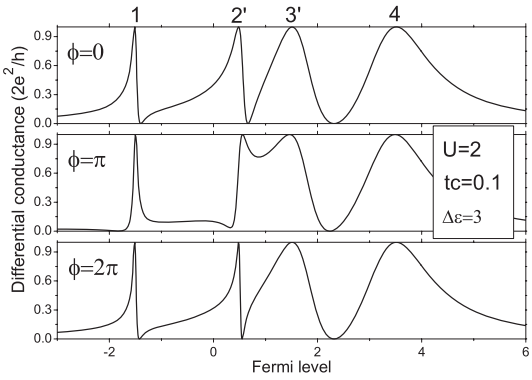

Figure 6. The conductance spectra versus Fermi level when $\Delta\varepsilon = 3$, $t_c = 0.1$, and $U = 2$. From top to bottom, $\phi = 4n\pi$, $(2n+1)\pi$, and $(2n+1)2\pi$. The other parameters taken for calculation are the same as figure 4.

the effective one-particle picture, can be well understood only invoking the Coulomb blockage mechanism. All results above can be similarly found in configuration 1, which will not be addressed repeatedly.

The interference between channels $2'$ and $3'$ responds to the magnetic flux ϕ in a period of 4π (figures 5 and 6). In particular, when an extra flux of π is added, the tail direction of the Fano peaks at 1, $2'$ or $3'$ is flipped, quite similar to the $\Delta\varepsilon = 0$ case in which configuration 1 is tuned to configuration 2. The line shape at $\phi = (2n+1)2\pi$ almost recovers that at $\phi = 4n\pi$ with slight variation in details. Compare with the $\Delta\varepsilon = 0$ case, where the magnetic tuning leads to the swap effect because of varying the effective broadening of two molecular states; here the widths of $2'$ and $3'$ are robust to magnetic tuning and depend only on $\Delta\varepsilon$, which resembles the parallel DQD without the inter-dot coupling.

4. Discussion and conclusions

Considering the small level spacing in the GaAs quantum dots in experiments by Holleitner *et al*, an electron may hop to the neighbour level before the above phenomena could be probed. We suggest further experiments be carried out in quantum dots with smaller radius R. For example, the typical experimental parameters are $U \cong 3.39$ meV, $\Delta\epsilon \cong 0.114$ meV, corresponding to a quantum dot with $R = 54$ nm [12], and $U = 2.95$ meV, $\Delta\epsilon = 0.308$ meV for a dot with $R = 60$ nm [16]. Assuming the GaAs quantum dot as a two-dimensional disc, U is proportional to R^{-1} while $\Delta\epsilon$ is proportional to R^{-2}. Keeping shrinking the dot size, we will eventually get $\Delta\epsilon \sim U$. We estimate that to observe the expected Fano effect in hybridized bands the radius of GaAs quantum dots should be around 2–6 nm, which is not an easy task for the present experimental configurations, but in principle possible. Other single-electron devices such as single-molecule transistors may also be chosen as candidates [31–34]. Being of small size, for instance the diameter of the C_{60} molecule is about 0.7 nm, the level spacings and charging energies in the systems are of the same order.

The conductance as a function of U in configuration 2 is shown in figure 7, in which four peaks denoted by the bright lines are respectively centred at $\varepsilon_0 - t_c$, $\varepsilon_0 + t_c + \frac{1}{2}(U - \sqrt{U^2 + 4t_c^2})$, $\varepsilon_0 - t_c + \frac{1}{2}(U + \sqrt{U^2 + 4t_c^2})$, and $\varepsilon_0 + t_c + U$. As mentioned above, when taking the many-body interaction into account, the resonant conductance peaks correspond to energy levels, for which an extra electron (the total number of electrons is $n + 1$) is introduced to the

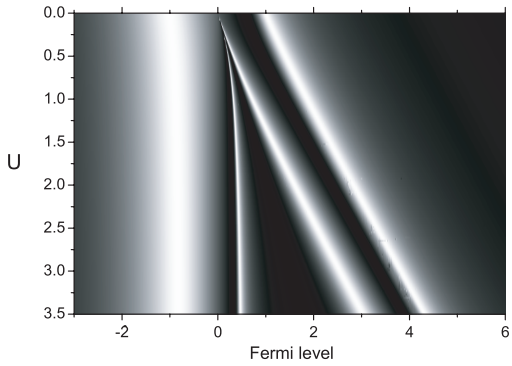

Figure 7. The conductance spectra versus U in configuration 2. The parameters taken for calculation are $\varepsilon_{1\sigma} = \varepsilon_{2\sigma} = 0$, $t_c = 1$, $U_1 = U_2 = U$, $\Gamma_1^L = \Gamma_1^R = 1$, $\Gamma_2^L = \Gamma_2^R = 0.15$.

n-electron system, with the peak position centred at $E_{n+1} - E_n$ [35, 41]. Here, the ground-state energy for n electrons in the isolated DCI, E_n (up to four in the present study), is as follows: $E_1 = \varepsilon_0 - t_c$, $E_2 = 2\varepsilon_0 + \frac{1}{2}(U - \sqrt{U^2 + 4t_c^2})$, $E_3 = 3\varepsilon_0 + U - t_c$, and $E_4 = 4\varepsilon_0 + 2U$. The peak positions at the DOS and conductance spectra we obtained comply with [41, 38–40], but disagree with results from the half-filling two-site Hubbard model: $2\varepsilon_0 + \frac{1}{2}(U - \sqrt{U^2 + 16t_c^2})$. The reason for the disagreement is simple, as the two-particle ground state in the two-site Hubbard model, which is superposed of the singlets as $\alpha(|\uparrow\rangle_1|\downarrow\rangle_2 - |\downarrow\rangle_1|\uparrow\rangle_2) + \beta(|\uparrow\downarrow\rangle_1|0\rangle_2 + |0\rangle_1|\uparrow\downarrow\rangle_2)$ [41, 42, 35], is forbidden by equation (11), where the coefficients α and β are determined by the ratio t_c/U. Therefore, the current approximation is justified only when U is much larger than t_c, which is exploited throughout the paper. The solution to this problem probably lies in solving the isolated DQD Green function $\mathbf{g}$ exactly, followed by including the self-energies due to leads by the Dyson equation, as has been done by Bułka *et al* in a series-coupled DQD system [35]. This involves self-consistently solving as many as 19 correlators, such as $\langle n_{1\sigma} n_{2\bar{\sigma}} \rangle$, $\langle d_{1\sigma}^\dagger d_{2\sigma} d_{1\bar{\sigma}}^\dagger d_{2\bar{\sigma}} \rangle$, $\langle d_{1\sigma}^\dagger d_{2\sigma} n_{1\bar{\sigma}} n_{2\bar{\sigma}} \rangle$, etc, which is beyond the task of the present paper.

In summary, within the Keldysh nonequilibrium Green function formalism and the equation of motion method, the transport through the parallel-coupled DQD system has been studied with an emphasis put on the intra-dot Coulomb repulsion on the Fano interference. By neglecting all spin-flip processes, two types of Fano interference are studied. When two quantum dots are degenerate, main results obtained in the noninteracting model can be reproduced for the Coulomb counterparts, such as flipping the direction of the asymmetric tail of Fano peaks and the swapping effect between DQD bands. When separation between two QD levels is large enough, the antibonding and the Coulomb blockade counterpart of the bonding states are mixed up, which may result in two new channels. The interference between them give rise to Fano resonances whose response to the external electrostatic and magnetic tuning is quite different from the no-U one.

Acknowledgments

We would like to acknowledge Hui Zhai, Zuo-zi Chen, Chao-xing Liu, and Zhen-Gang Zhu for helpful discussions. This work is supported by the Natural Science Foundation of China (grant No 10374056, 10574076), the MOE of China (grant No 2002003089), and the Program of Basic Research Development of China (grant No 2001CB610508).

References

[1] Fano U 1961 *Phys. Rev.* **124** 1866
[2] Kouwenhoven L P, Markus C M, McEuen P L, Tarucha S, Westervelt R M and Wingreen N S 1997 *Mesoscopic Electon Transport* (*NATO Advanced Study Institutes, Ser. E* vol 345) ed L L Sohn, L P Kouwenhoven and G Schön (Dordrecht: Kluwer)
[3] Göres J, Goldhaber-Gordon D, Heemeyer S, Kastner M A, Shtrikman H, Mahalu D and Meirav U 2000 *Phys. Rev.* B **62** 2188
[4] Zacharia I G, Goldhaber-Gordon D, Granger G, Kastner M A, Khavin Y B, Shtrikman H, Mahalu D and Meirav U 2001 *Phys. Rev.* B **64** 155311
[5] Kobayashi K, Aikawa H, Katsumoto S and Iye Y 2002 *Phys. Rev. Lett.* **88** 256806
[6] Kobayashi K, Aikawa H, Katsumoto S and Iye Y 2003 *Phys. Rev.* B **68** 235304
[7] Johnson A C, Marcus C M, Hanson M P and Gossard A C 2004 *Phys. Rev. Lett.* **93** 106803
[8] Adair R K, Bockelman C K and Peterson R E 1949 *Phys. Rev.* **76** 308
[9] Fano U and Cooper J W 1965 *Phys. Rev.* **137** A1364
[10] Cerdeira F, Fjeldly T A and Cardona M 1973 *Phys. Rev.* B **8** 4734
[11] Faist J, Capasso F, Sirtori C, West K W and Pfeiffer L N 1997 *Nature* **390** 589
[12] Holleitner A W, Decker C R, Qin H, Eberl K and Blick R H 2001 *Phys. Rev. Lett.* **87** 256802
[13] Holleitner A W, Blick R H, Hüttel A K, Eberl K and Kotthaus J P 2002 *Science* **297** 70
[14] Holleitner A W, Blick R H and Eberl K 2003 *Appl. Phys. Lett.* **82** 1887
[15] Blick R H, Hüttel A K, Holleitner A W, Höhberger E M, Qin H, Kirschbaum J, Weber J, Wegscheider W, Bichler M, Eberl K and Kotthaus J P 2003 *Physica* E **16** 76
[16] Chen J C, Chang A M and Melloch M R 2004 *Phys. Rev. Lett.* **92** 176801
[17] Ladron de Guevara M L, Claro F and Orellana P A 2003 *Phys. Rev.* B **67** 195335
[18] Kang K and Cho S Y 2004 *J. Phys.: Condens. Matter* **16** 117
[19] Bai Z-M, Yang M-F and Chen Y-C 2004 *J. Phys.: Condens. Matter* **16** 2053
[20] Orellana P A, Ladrón de Guevara M L and Claro F 2004 *Phys. Rev.* B **70** 233315
[21] Lu H, Lü R and Zhu B F 2005 *Phys. Rev.* B **71** 235320
[22] Dong B and Lei X L 2002 *Phys. Rev.* B **65** 241304(R)
[23] Ding G H, Kim C K and Nahm K 2005 *Phys. Rev.* B **71** 205313
[24] Tanaka Y and Kawakami N 2005 *Phys. Rev.* B **72** 085304 (*Preprint* cond-mat/0510253)
[25] Zhang G M, Lü R, Liu Z R and Yu L 2005 *Phys. Rev.* B **72** 073308
[26] Dong B, Djuric I, Cui H L and Lei X L 2004 *J. Phys.: Condens. Matter* **16** 4303
[27] Chi F and Li S S 2005 *J. Appl. Phys.* **97** 123704
[28] Loss D and DiVincenzo D P 1998 *Phys. Rev.* A **57** 120
[29] DiVincenzo D P 1996 *Preprint* cond-mat/9612126 ; also in Ref. [2]
[30] Clerk A A, Waintal X and Brouwer P W 2001 *Phys. Rev. Lett.* **86** 4636
[31] Park H, Park J, Lim A, Anderson E, Alivisatos A and McEuen P 2000 *Nature* **407** 57
[32] Park J, Pasupathy A N, Goldsmith J I, Chang C, Yaish Y, Petta J R, Rinkowski M, Sethna J P, Abruña H D, McEuen P L and Ralph D C 2002 *Nature* **417** 722
[33] Liang W, Shores M P, Bockrath M, Long J R and Park H 2002 *Nature* **417** 725
[34] Yu L H and Natelson D 2004 *Nano Lett.* **4** 79
[35] Bułka B R and Kostyrko T 2004 *Phys. Rev.* B **70** 205333
[36] Meir Y and Wingreen N S 1992 *Phys. Rev. Lett.* **68** 2512
[37] Haug H and Jauho A P 1996 *Quantum Kinetics in Transport and Optics of Semiconductors* (Berlin: Springer)
[38] Pals P and Mackinnon A 1996 *J. Phys.: Condens. Matter* **8** 5401
[39] You J Q and Zheng H Z 1999 *Phys. Rev.* B **60** 13314
[40] Lamba S and Joshi S K 2000 *Phys. Rev.* B **62** 1580
[41] Klimeck G, Chen G and Datta S 1994 *Phys. Rev.* B **50** 2316
[42] Ziesche P, Gunnarsson O, John W and Beck H 1997 *Phys. Rev.* B **55** 10270
[43] Borda L, Zaránd G, Hofstetter W, Halperin B I and von Delft J 2003 *Phys. Rev. Lett.* **90** 026602
[44] Lopez R, Sánchez D, Lee M, Choi M-S, Simon P and Hur K L 2005 *Phys. Rev.* B **71** 115312
[45] Sakano R and Kawakami N 2005 *Phys. Rev.* B **72** 085303